COMMUNICATIONS CHEMISTRY

ARTICLE

https://doi.org/10.1038/s42004-019-0132-5 OPEN

Theoretical study of FMO adjusted C-H cleavage and oxidative addition in nickel catalysed C-H arylation

Tao Zhang[1], Song Liu[1], Lei Zhu[1], Fenru Liu[1], Kangbao Zhong[1], Ying Zhang[1], Ruopeng Bai[1] & Yu Lan[1,2]

Nickel catalysis has recently emerged as an important addition to the suite of transition metal-catalysed C-H bond functionalization methods. Here we report density functional theory calculations to elucidate the mechanism of Ni(II)-catalysed C–H arylation with a diaryliodonium salt or a phenyliodide. The effect of the choice of oxidant on the order of oxidative addition and C–H bond cleavage is investigated. When the active catalyst is oxidized by the diaryliodonium salt oxidant, C–H bond cleavage occurs to give an alkyl-aryl-Ni (IV) species. Conversely, the relatively weak oxidant phenyliodide leads to an alternative reaction sequence. The active catalyst first undergoes C–H bond cleavage, followed by oxidative addition of the phenyliodide to give a Ni(IV) species. Frontier molecular orbital analysis demonstrates that the reaction sequence of oxidative addition and C–H bond cleavage is determined by the unoccupied C_{aryl}–I bond antibonding orbital level of the oxidant.

[1] School of Chemistry and Chemical Engineering, Chongqing Key Laboratory of Theoretical and Computational Chemistry, Chongqing University, Chongqing 400030, China. [2] College of Chemistry and Molecular Engineering, Zhengzhou University, Zhengzhou 450001, P. R. China. Correspondence and requests for materials should be addressed to R.B. (email: ruopeng@cqu.edu.cn) or to Y.L. (email: lanyu@cqu.edu.cn)

Over the past few decades, transition-metal-catalysed C–H bond functionalization reactions have been widely used in synthetic chemistry to construct C–C and C–heteroatom bonds[1–6]. Despite the great advances in this field, a large number of transformations are yet to be discovered and some inherent limitations remain, such as the limited range of compatible substrates and the C–H bond functionalization site selectivity. It is noteworthy that transition-metal catalysts, such as palladium[7,8], rhodium[9–11], ruthenium[12,13] and nickel[14–17] catalysts, are critical for many of these transformations, and they often exhibit remarkable reactivity. Among these transition-metal catalysts, nickel complexes are often more sustainable and economical than palladium, rhodium and ruthenium complexes[18,19]. Furthermore, the bond dissociation energies of C–Ni bonds are usually lower than those of C–Pd bonds, which provides the opportunity to develop sequential C–Ni bond functionalization processes for the construction of C–C or C–X bonds[5,20–23].

In 2011, Chatani and co-workers reported the first Ni-catalysed ortho-C–H bond functionalization directed by 2-pyridinylmethylamine, which was found to efficiently promote the transformation[24]. Subsequently, 8-aminoquinoline, another *N*,*N*-bidentate directing group, was also reported by Chatani's group for the Ni-catalysed ortho-alkylation of benzamide derivatives[25]. A variety of Ni-catalysed C–H bond functionalization reactions have since been extensively explored by taking advantage of *N*,*N*-bidentate directing groups[26–38].

The introduction of *N*,*N*-bidentate directing groups is a helpful means of loading the substrate and specifying the C–H bond cleavage site, and 8-aminoquinoline has been extensively used as a directing group in Ni-catalysed C–H bond functionalization. As an example, Chatani's group reported two series of Ni(II)-catalysed arylation reactions involving C–H bonds in aliphatic amides (Fig. 1)[39,40]. In these reactions, a strongly oxidizing diaryliodonium salt (Fig. 1a) or a relatively weakly oxidizing aryl halide (Fig. 1b) is used as an efficient aryl source. In both cases, 8-aminoquinoline acts as a bidentate directing group and coordinates in an *N*, *N* fashion to the Ni centre. In addition to the proposed mechanism, five subsequent processes are involved in the catalytic cycle of the aforementioned reactions: These include coordination of the directing group, C–H bond cleavage, oxidative addition, reductive elimination, and protonation. Although it is widely held that oxidative addition occurs immediately after C–H bond cleavage in transition-metal catalysed C–H bond functionalization reactions[41], the order of these two steps is still not certain. In addition, the sequence of these two steps could potentially affect the mechanism of the following steps due to the change in the oxidation state of the metal.

Our group has previously reported various mechanistic studies of transition-metal-catalysed C–H bond functionalization reactions[42–48]. In most cases, C–H bond cleavage by a metal having a low oxidation state occurs before oxidative addition, but this reaction sequence can be reversed. As an example, in the case of the catalytic cycle of $Rh_2(OAc)_4$-catalysed oxidation of toluene[49], the $Rh_2(OAc)_4$ catalyst is first oxidized by Selectfluor (1-chloromethyl-4-fluoro-1,4-diazoniabicyclo[2.2.2]octane bis(tetrafluoroborate)), followed by C–H bond cleavage with the resulting Rh(III)–Rh(III) intermediate. This unusual mechanism is due to the strong oxidizing ability of Selectfluor, which accelerates the oxidative addition step and stabilizes the high valence metallic intermediates to promote the C–H bond cleavage step. Based on these considerations, we believe that the order of C–H bond cleavage and oxidative addition is important and needs to be clarified by a mechanistic study of Ni-catalysed C–H bond functionalization reactions.

Here, we focus on the mechanism for the Ni(II)-catalysed arylation of C–H bonds in aliphatic amides with the aim of addressing some of the ambiguity associated with the reaction sequence. Although the mechanism of Ni(II)-catalysed arylation of C–H bonds in aliphatic amides has been investigated in several computational and experimental studies[50–52], a clear understanding of the order of C–H bond cleavage and oxidative addition is still elusive, even though this knowledge is important in assessing these transformations. Therefore, in the present study, we perform density functional theory (DFT) calculations to

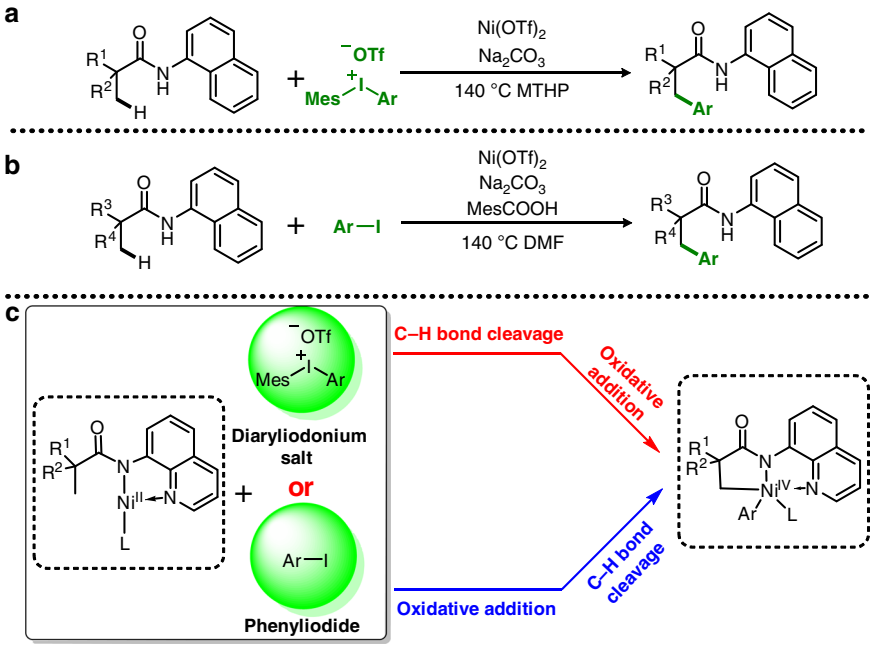

Fig. 1 Nickel-catalysed C–H arylation. **a** Ni(II)-catalysed C–H bond arylation with the diaryliodonium salt oxidant. **b** Ni(II)-catalysed the C–H bond arylation with the phenyliodide oxidant. **c** Proposed mechanism of Ni(II)-catalysed C–H arylation with a diaryliodonium salt or a phenyliodide

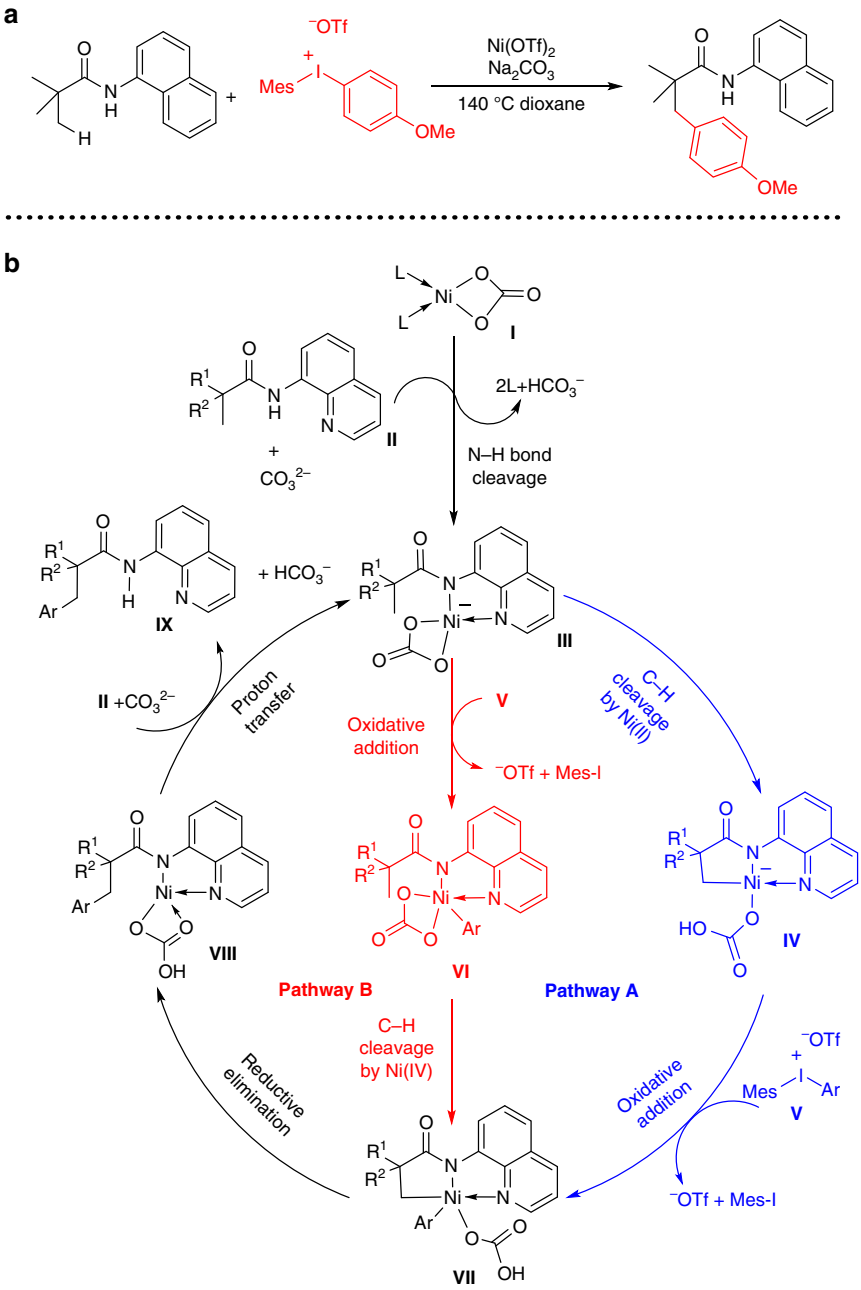

Fig. 2 C–H arylation using a diaryliodonium salt. **a** Model reaction based on the Ni(II)-catalysed C–H bond arylation of an aliphatic amides with a diaryliodonium salt. **b** Plausible mechanisms for the Ni(II)-catalysed C–H bond arylation of an aliphatic amides with a diaryliodonium salt

examine differences between the mechanisms of Ni(II)-catalysed C–H bond arylation reactions with a diaryliodonium salt or with a phenyliodide as the oxidant (Fig. 1c). An additional goal is to determine whether these reactions begin with C–H cleavage or proceed by an alternative sequence starting with oxidative addition. Most importantly, our intent is to find the factors determining the order of C–H cleavage and oxidative addition.

Results

Ni(II)-catalysed C–H bond arylation of aliphatic amides with a diaryliodonium salt. Our prior work has shown that the use of strong oxidants may change the reaction order of the C–H cleavage and oxidative addition steps in Rh-catalysed C–H bond functionalization reactions. Therefore, we first investigated the mechanism associated with the Ni(II)-catalysed C–H bond arylation of aliphatic amides, employing a diaryliodonium salt. The process using *N*-(quinolin-8-yl)pivalamide previously reported by Chatani's group was selected as a model reactions (Fig. 2a). As shown in Fig. 2b, two plausible pathways were considered during our computational modelling of such reaction. Based on a prior mechanistic studies of Ni(II)-catalysed C–H bond functionalization reactions, pathway A (in blue) was first considered. Initially, cleavage of the N–H bond cleavage in aliphatic amide **II** with Na_2CO_3 and Ni(II) catalyst **I**, which is generated from $Ni(OTf)_2$ by dissociation and ligand exchange reactions in the presence of Na_2CO_3 and solvent, gives Ni(II) complex **III**. Carbonate-assisted cleavage of the C–H bond in complex **III** then generates alkyl-Ni intermediate **IV**, which subsequently undergoes oxidative addition with diaryliodonium salt **V** to give Ni(IV) intermediate **VII**. However, the alternate pathway B (in red) should also be considered. In this mechanism,

oxidative addition of Ni(II) complex **III** to diaryliodonium salt **V** occurs first, to give Ni(IV) intermediate **VI**, owing to the strong oxidizing nature of diaryliodonium salt **V**. Subsequently, carbonate-assisted cleavage of the C–H bond in Ni(IV) intermediate **VI** provides the common Ni(IV) intermediate **VII**. Finally, proton exchange between aliphatic amide **II** and Ni(II) intermediate **VIII**, which is generated by reductive elimination of Ni(IV) intermediate **VII**, regenerates active Ni(II) complex **III**. DFT calculations were performed to investigate Ni(II)-catalysed C–H bond arylation of aliphatic amides with a diaryliodonium salt.

In the theoretical calculations, the reaction with *N*-(quinolinyl) pivalamide was chosen as the model reaction (Fig. 2a), and the calculated free energy profile for the formation of active catalytic species **6** is shown in Fig. 3. The stable quinolone-coordinated Ni (II) intermediate **3** is generated after ligand exchange between *N*-(quinolinyl)pivalamide **2** and Ni(II) catalyst **1**. The N–H bond cleavage step then occurs via six-membered-ring transition state **4-ts** to form amidonickel intermediate **5**. The free energy for this step beginning from intermediate **3** is 23.7 kcal mol^{-1}, and so this process could easily occur at a reaction temperature of 140 °C. Counterion exchange of intermediate **5** with a carbonate ion then gives active catalytic species **6**.

Based on previous theoretical studies[33,53–55], oxidative addition is generally considered to occur after C–H bond cleavage in the majority of Ni(II)-catalysed C–H bond functionalization reactions. With this in mind, we initially calculated the free energy profile for pathway A as shown in Fig. 2b, and the resulting free energy profile is presented in Fig. 4 (blue pathway). In Fig. 4, the free energy of the anionic Ni(II) carbonate complex **6**, which is generated upon the addition of $Ni(OTf)_2$ via N–H cleavage and counterion exchange with a carbonate ion in the presence of *N*-(quinolin-8-yl)pivalamide and Na_2CO_3, is set to a relative value of zero. In pathway A, carbonate-assisted cleavage of the C–H bond in complex **6** occurs via the concerted metalation-deprotonation (CMD)-type transition state **7-ts** with a free energy of 27.6 kcal mol^{-1} to reversibly form alkyl-Ni(II) intermediate **8**. The geometry of transition state **7-ts** shows that the length of the Ni–H bond is 1.83 Å (Fig. 4), which indicates a weak interaction between Ni and the reacting H atom. Coordination between intermediate **8** and diaryliodonium salt **9** then gives the more stable oxygen-coordinated diaryliodonium intermediate **10** in an exothermic process that releases 3.5 kcal mol^{-1} of free energy, accompanied by dissociation of the OTf^- annion. Subsequent oxidation then occurs via six-membered-ring-type transition state

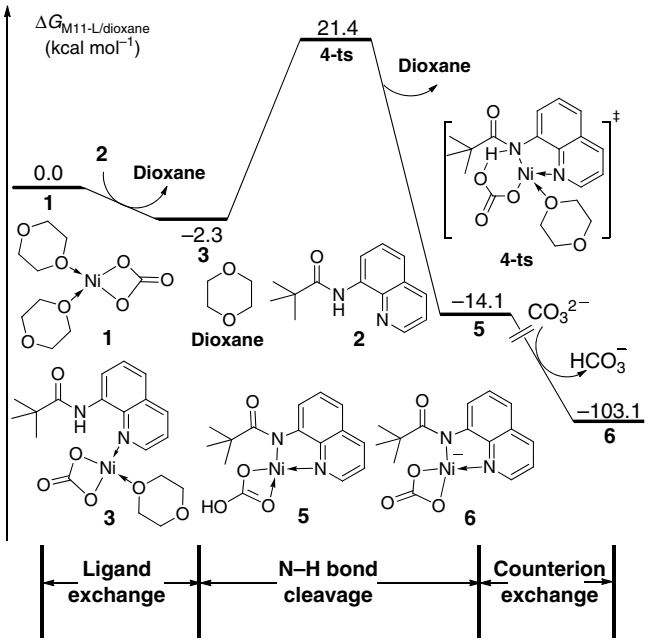

Fig. 3 Free energy profile for catalyst formation with a diaryliodonium salt. Free energy profile for the formation of active catalytic species **6** in Ni(II)-catalysed C–H bond arylation with a diaryliodonium salt. Relative energy changes are in kcal mol^{-1} and were calculated at the M11-L/6-311+G(d) level in dioxane solvent

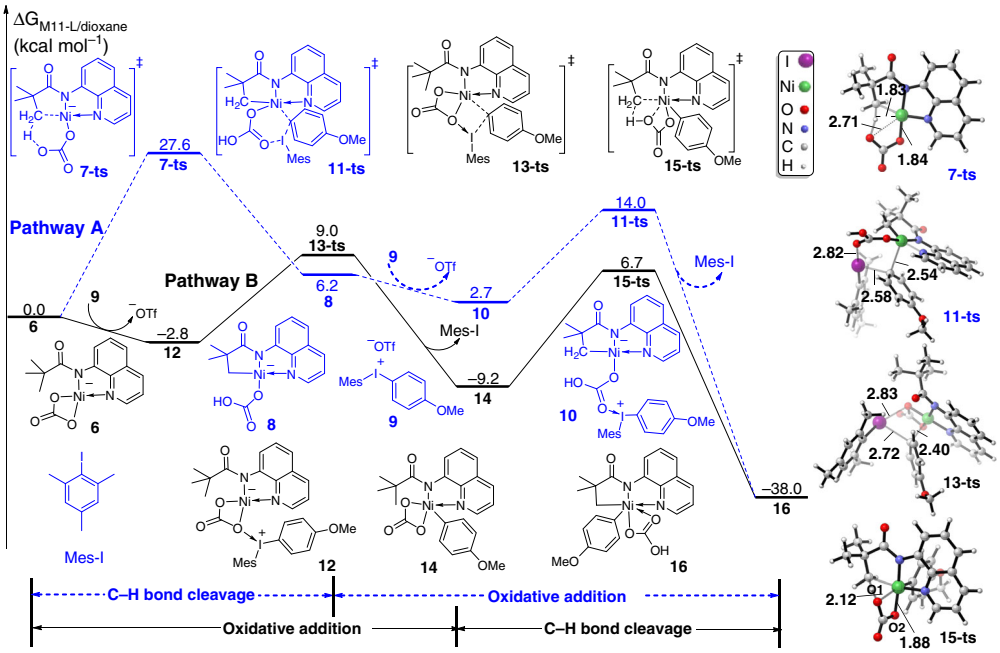

Fig. 4 Free energy of C–H metalation with a diaryliodonium salt. Free energy profiles of C–H bond cleavage and oxidative addition steps of Ni(II)-catalysed C–H bond arylation with a diaryliodonium salt. Relative energy changes are in kcal mol^{-1} and were calculated at the M11-L/6-311+G(d) level in dioxane solvent. Optimized geometries of transition states **7-ts**, **11-ts**, **13-ts**, and **15-ts**. The bond lengths are in angstroms

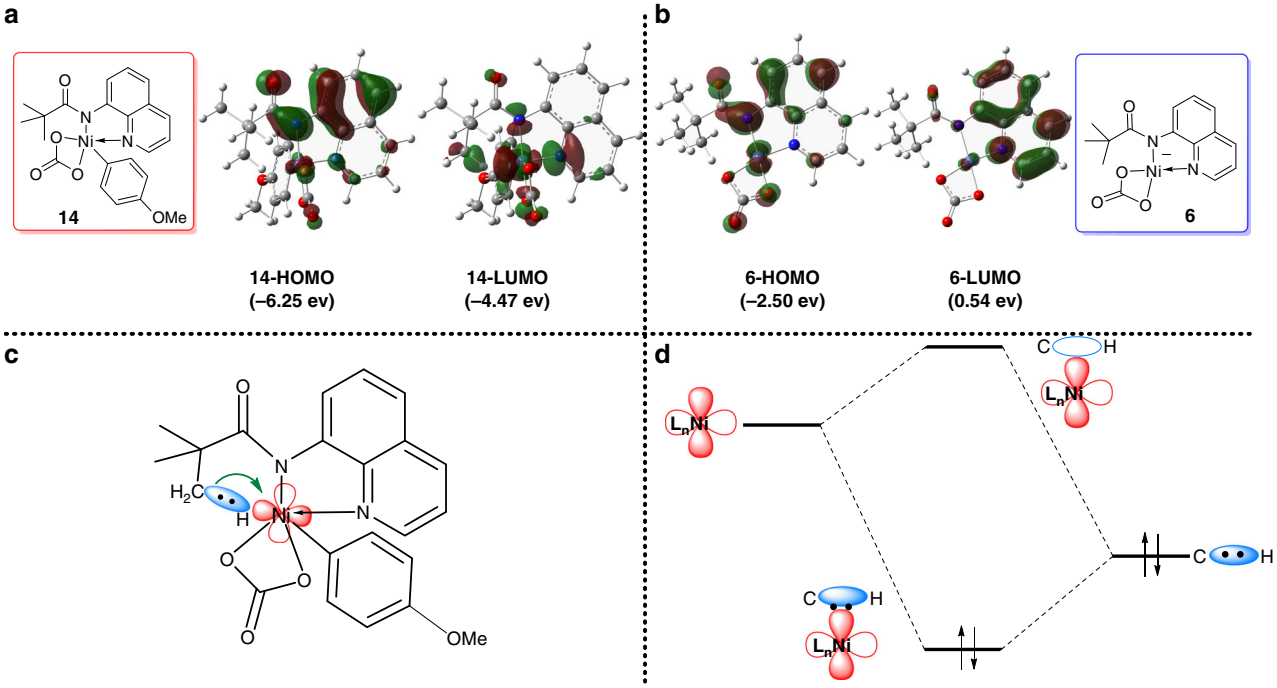

Fig. 5 FMO analysis. **a** FMO analysis of **14**. **b** FMO analysis of **6**. **c** Model of the interaction between Ni and the C–H bond in **14**. **d** FMO diagram of the C–H bond cleavage step

11-ts with the release of 2-iodo-1,3,5-trimethylbenzene (MesI) to give aryl-Ni(IV) species **16**. The calculated free energy for this process is only 11.3 kcal mol^{-1}. The geometry of transition state **11-ts** shows that the bond lengths of the C_{aryl}–I and C_{aryl}–Ni bonds being broken and formed are 2.58 and 2.54 Å, respectively, which indicates that C_{aryl}–I bond breaking occurs as the C_{aryl}–Ni bond forms.

According to the above computational results, in pathway A, the oxidative addition step proceeds more readily than the C–H bond cleavage step. Therefore, we investigated another possible pathway starting with oxidative addition followed by C–H bond cleavage (pathway B, the black pathway in Fig. 4). In pathway B, coordination of diaryliodonium salt **9** replaces OTf^- in Ni(II) complex **6** to form neutral Ni(II) intermediate **12**, and this process is exothermic by 2.8 kcal mol^{-1}. Oxidative addition of Ni (II) intermediate **12** then proceeds rapidly via concerted six-membered-type transition state **13-ts** with the concomitant release of MesI, This process requires an activation free energy of only 11.8 kcal mol^{-1} to produce the more stable aryl-Ni(IV) intermediate **14**. The activation free energy associated with the oxidative addition of intermediate **12** is only 0.5 kcal mol^{-1} higher than the corresponding process in pathway A, indicating that oxidative addition may occur first in this reaction sequence. Following the oxidative addition step, carbonate-assisted C–H bond cleavage of intermediate **14** generates the common Ni(IV) intermediate **16** through concerted four-membered-ring transition state **15-ts**. It is noteworthy that the energy barrier for C–H cleavage from Ni(IV) intermediate **14** is 15.9 kcal mol^{-1}, which is 11.8 kcal mol^{-1} lower than the corresponding process involving Ni(II) intermediate **6**, indicating that C–H activation mediated by Ni in a high oxidation state (IV) is more rapid compared with that mediated by Ni(II). The difference in the energy barriers for C–H bond cleavage processes can be understood by considering the geometries of the corresponding transition states **7-ts** and **15-ts**. As shown in Fig. 4, the geometry of **7-ts** is square planar because the formal oxidative state of Ni is +2. Therefore, only one oxygen atom of the carbonate ion coordinates with Ni, and the calculated Ni–O distances were calculated as 2.71 and 1.84 Å. The two formal-negative charges of the carbonate moiety are only partially stabilized by the Ni atom, resulting in a high-relative free energy. In the other case, the calculated geometry of transition state **15-ts** is octahedral because the formal oxidative state of Ni is +4. Therefore, both of the oxygen atoms of the carbonate ion coordinate with the Ni centre. The Ni–O1 and Ni–O2 bond distances are 2.12 and 1.88 Å, respectively, confirming a strong interaction between the carbonate ion and Ni. Therefore, the energy barrier for C–H cleavage is lower.

The effect of the oxidation state of Ni can be elucidated by frontier molecular orbital (FMO) analysis of reaction intermediates **6** and **14**. The FMOs of intermediate **14** are shown in Fig. 5a. The calculated geometry for intermediate **14** is square pyramidal, which suggests that the Ni centre has a vacancy because of its +4 oxidation state. Therefore, the lowest unoccupied molecular orbital (LUMO) of intermediate **14** is a 3d orbital of the Ni atom. Interestingly, a 3d orbital character is clearly present in the calculated LUMO. Part of the σ-bond orbital component of the reacting C–H bond also appears in the LUMO of intermediate **14**, demonstrating that there is a d_{Ni}–σ_{C-H} interaction in this species. The contributions of the orbital interactions were examined by generating the qualitative schematic FMO diagrams is shown in Fig. 5c, d. In the C–H activation mode, the occupied σ_{C-H} orbital would be expected to interact with an unoccupied Ni *d* orbital of Ni to activate the corresponding C–H bond. The antibonding orbital of this interaction is evidently the LUMO of intermediate **14**, showing a significant d_{Ni}–σ_{C-H} interaction. In this manner, the C–H bond in intermediate **14** is activated, thus lowering activation energy associated with C–H bond cleavage via transition state **15**. These results confirm that the d_{Ni}–σ_{C-H} orbitals overlap, which would generate the C-Ni bond, is the driving force of the C–H activation step. This C–H bond cleavage proceeds via a base-assisted internal electrophilic-type substitution (BIES) process in the presence of high oxidation state Ni(IV) centre[56,57]. Figure 3b presents the FMOs of intermediate **6**, which is square planar and contains fully coordinated 16e$^-$ Ni(II).

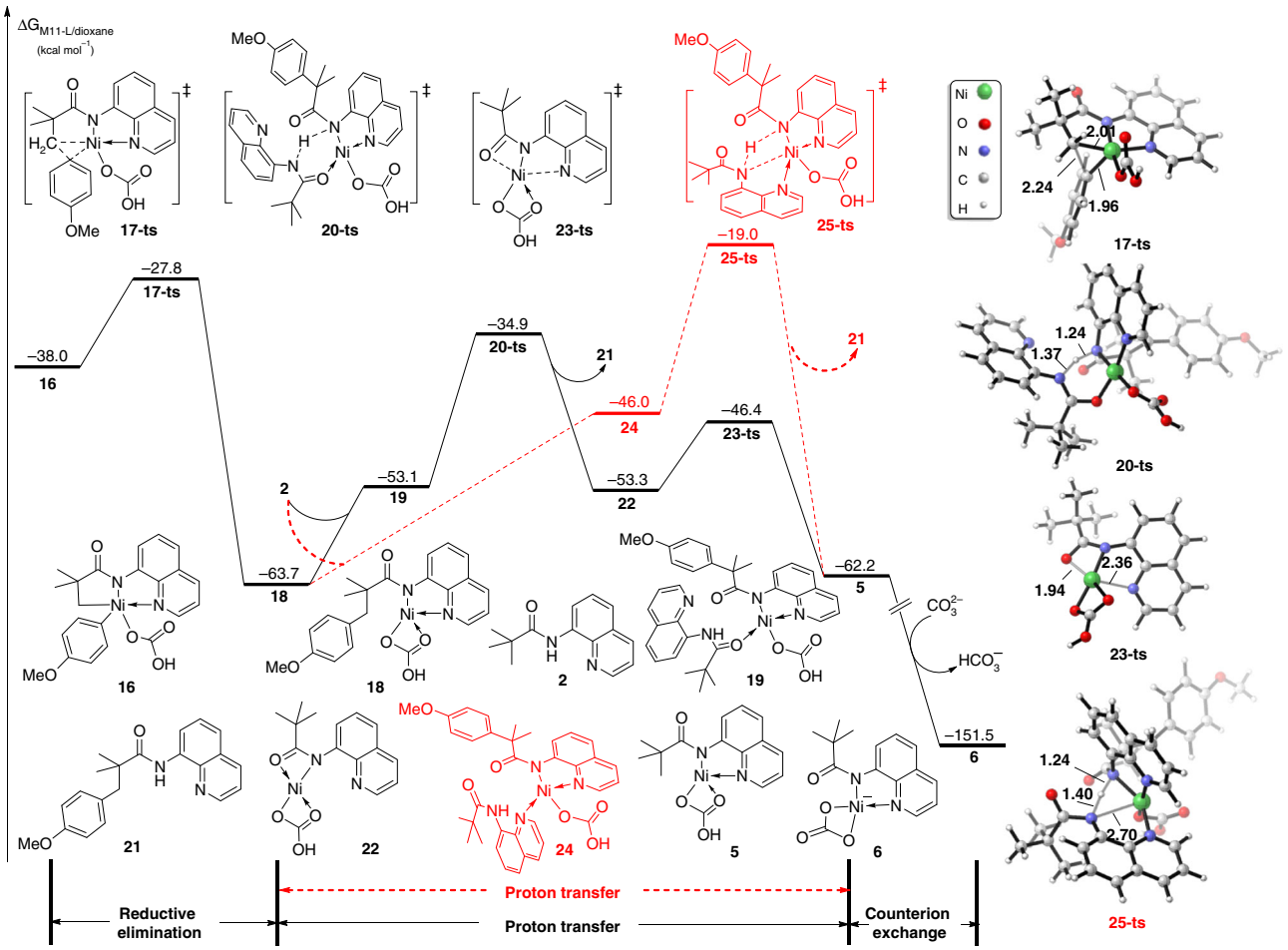

Fig. 6 Free energy profile for C–H arylation with a diaryliodonium salt. The free energy profile for the reductive elimination, proton transfer, and counterion exchange steps during Ni(II)-catalysed C–H bond arylation with a diaryliodonium salt. Relative energy changes are in kcal mol^{-1} and were calculated at the M11-L/6-311+G(d) level in dioxane solvent. Optimized geometries of transition states **17-ts**, **20-ts**, **23-ts**, and **25-ts**. The bond lengths are in angstroms

Therefore, the Ni centre in this species does not have a vacancy. The FMO calculation results for this intermediate also shows the absence of a d_{Ni}–σ_{C-H} interaction in intermediate **6**, which rules out the BIES mechanism. When CMD type C–H cleavage occurs from intermediate **6**, one coordinated oxygen atom should dissociate to generate a vacancy for the reacting C–H bond, which leads to a high activation barrier.

On this basis, it is apparent that the C–H bond cleavage step is promoted by the high-oxidation state metal centre generated during the oxidative addition. The results in Fig. 4 show that pathway B is the preferred mechanism, and proceeds through ligand exchange with the substrate, oxidative addition by the diaryliodonium salt, and a BIES type C–H bond cleavage to give the Ni(IV) metallacycle complex **16**. These same computations were performed using a number of different substituted aliphatic amides and diaryliodonium salt oxidants (see Supplementary Fig. 5 for details). The results show that the order of the oxidative addition and C–H bond cleavage steps in each of these reactions is the same as in the model reaction described herein. These results provide further support for the mechanisms proposed for Ni(II)-catalysed C–H bond arylation with a diaryliodonium salt.

Figure 6 presents the free energy profile for the reductive elimination, proton transfer, and ligand exchange steps during the Ni(II)-catalysed C–H bond arylation of aliphatic amides with a diaryliodonium salt. Following the formation of Ni(IV) intermediate **16**, reductive elimination rapidly proceeds to form a new C_{alkyl}–C_{aryl} bond via three-membered-ring transition state **17-ts** with an energy barrier of only 10.2 kcal mol^{-1}, This, in turn, leads to the irreversible generation of intermediate **18**. Coordination of the oxygen atom of the amino group of another **2** molecule gives intermediate **19**, and this step is endergonic by 10.6 kcal mol^{-1}. Proton exchange between the reactant and product subsequently occurs via transition state **20-ts** with an overall activation free energy of 28.8 kcal mol^{-1} to form aminonickel intermediate **22**. Ligand exchange rapidly occurs via transition state **23-ts** to form quinolone-coordinated aminonickel **5**, which promotes another catalytic cycle. The computational results indicate that the proton exchange step is the rate-limiting step of the overall catalytic cycle. We also considered a quinolone-directed proton exchange process via transition state **25-ts**, but the relative free energy of this transition state was found to be much higher than that of **20-ts**.

According to the above computational results, a reasonable reaction pathway for the Ni(II)-catalysed C–H bond arylation of an aliphatic amides with a diaryliodonium salt can be proposed. In this mechanism, the coordination and deprotonation–amination of *N*-(quinolinyl)pivalamide **2** with Ni(CO_3) followed by counterion exchange with the carbonate ion generates aminonickel intermediate **6**, which is the active catalyst in the catalytic cycle. Oxidative addition with diaryliodonium salt **9** generates aryl-Ni(IV) species **14**, which undergoes BIES type C–H bond cleavage to form alkyl-aryl-Ni(IV) species **16**. Reductive elimination then forms the new C_{aryl}–C_{alkyl} bond. Active catalyst **6** can be regenerated by proton exchange with release of arylation product **21**, which is considered

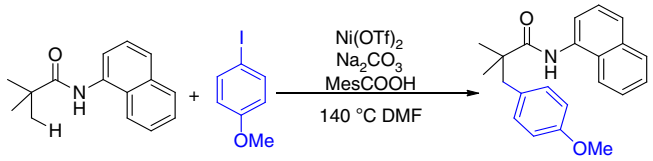

Fig. 7 C–H arylation with phenyliodide. Model reaction for Ni(II)-catalysed arylation of C–H bonds in aliphatic amides with a phenyliodide

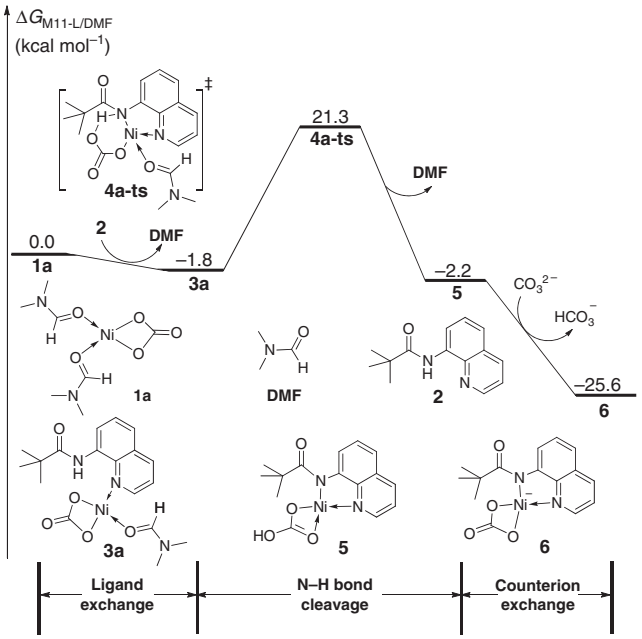

Fig. 8 Free energy profile for catalyst formation with phenyliodide. The free energy profile for the formation of active catalytic species 6 during the Ni (II)-catalysed C–H bond arylation of an aliphatic amides with a phenyliodide. Relative energy changes are in kcal mol^{-1} and were calculated at the M11-L/6-311+G(d) level in DMF solvent

to be the rate-determining step of the entire catalytic cycle. The computational results demonstrate that oxidative addition with a diaryliodonium salt occurs before C–H bond cleavage in this particular reaction, which is different from previous mechanisms proposed for this reaction based on experimental data. These theoretical calculations also show that, compared with Ni(II), C–H cleavage mediated by Ni(IV) is much easier, while the FMO analysis confirms that this step involves a BIES mechanism.

Mechanistic study of Ni(II)-catalysed C–H bond arylation with a phenyliodide. The mechanistic study of arylation with a diaryliodonium salt described in the preceding section indicate that the use of a strongly oxidizing diaryliodonium salt as the aryl source can rapidly generates a Ni(IV) species, followed by carbonate-assisted C–H bond cleavage. Based on these results, we decided to examine the reaction pathway in the case that a relatively weak oxidizing aryl source was employed in place of the diaryliodonium salt in Ni-catalysed C–H bond arylation. Thus, we performed additional calculations focusing on the mechanism of the Ni(II)-catalysed C–H bond arylation of an aliphatic amides with a phenyliodide (Fig. 7). Based on experimental observations, the added $Ni(OTf)_2$ and Na_2CO_3 react to form $Ni(CO_3)$, which is considered to act as the pre-catalyst in this reaction. Catalyst loading process also occurs through coordination of *N*-(quinolinyl)pivalamide **2** followed by carbonate-assisted N–H bond cleavage and counterion exchange with the carbonate ion to form active catalytic species **6**. As shown in Fig. 8, the calculated activation free energy of the N–H bond cleavage step using DMF as the solvent is 23.1 kcal mol^{-1} solvent, which is close to that in dioxane solvent (Supplementary Fig. 2).

DFT calculations were performed to investigate the transformation of intermediate **6** during the Ni(II)-catalysed arylation of C–H bonds in aliphatic amides with a phenyliodide. The preceding study of the corresponding reaction with a diaryliodonium salt suggested that the oxidative addition step with a phenyliodide may occur prior to C–H bond cleavage in this case. Therefore, oxidative addition of the phenyliodide followed by carbonate-assisted C–H bond cleavage was initially considered to determine the manner in which Ni(IV) intermediate **16** was generated. As shown in Fig. 9, the oxidative addition of intermediate **6** with phenyliodide **7a** goes through transition state **8a-ts** to form aryl-Ni(IV) complex **9a**, with an activation free energy of 41.3 kcal mol^{-1}. The geometry of intermediate **9a** is octahedral, and so an iodide anion dissociates to form square-pyramidal intermediate **10a** before C–H cleavage. Carbonate-assisted C–H bond cleavage then occurs via concerted metallation–deprotonation (CMD)-type transition state **11a-ts**. The overall activation free energy for this step is 46.0 kcal mol^{-1}, and so this pathway can be ruled out because of the high activation free energy.

We also considered the reaction pathway for carbonate-assisted C–H bond cleavage followed by oxidative addition. From intermediate **6**, carbonate-assisted C–H cleavage occurs via CMD-type transition state **7-ts** with a free energy barrier of only 24.4 kcal mol^{-1} to form alkyl-Ni(II) species **8**. The relative free energy of **8** is only 5.0 kcal mol^{-1} higher than that of intermediate **6**. Oxidative addition of **7a** to **8** then occurs via three-membered-ring-type transition state **12a-ts** with a free energy barrier of 26.1 kcal mol^{-1}. The computational results show that oxidative addition of phenyliodide **7a** is the rate-determining step for the whole-catalytic cycle. The overall activation free energy of this step is 31.1 kcal mol^{-1}, which is coincident with the experimental temperature (140 °C).

DFT calculations demonstrated that the use of phenyliodide as the oxidant in Ni-catalysed arylation, results in a pathway similar to that shown in blue pathway in Fig. 2b. This catalytic cycle starts from amino-Ni(II) species **6** and carbonate-assisted C–H bond cleavage followed by oxidative addition with the phenyliodide gives aryl-alkyl-Ni(IV) intermediate **16**. Rapid reductive elimination and counterion exchange then regenerate active catalyst **6** (the computational details concerning the regeneration of **6** are summarized in Supplementary Fig. 1). The transformations of a number of differently substituted aliphatic amides and phenyliodide oxidants were also examined (see Supplementary Fig. 6 for details). These results provide further support for the mechanisms proposed for Ni(II)-catalysed C–H bomjknd arylation with a phenyliodide derivative.

Important factors affecting oxidative addition with different arene sources. According to the above calculations, in a mechanism involving formation of active catalyst **6**, the order of the subsequent oxidative addition and C–H bond cleavage can be reversed by using different oxidants. Employing a strongly oxidizing diaryliodonium salt as the oxidant is favourable for oxidative addition followed by carbonate-assisted C–H bond cleavage. In contrast, using a relatively weakly oxidizing aryliodine as the oxidant results in carbonate-assisted C–H bond cleavage followed by oxidative addition.

Based on the mechanism studies, we wondered what factors of the oxidant are important in Ni(II)-catalysed C–H arylation reactions. Thus, we performed a further study of the FMOs of the

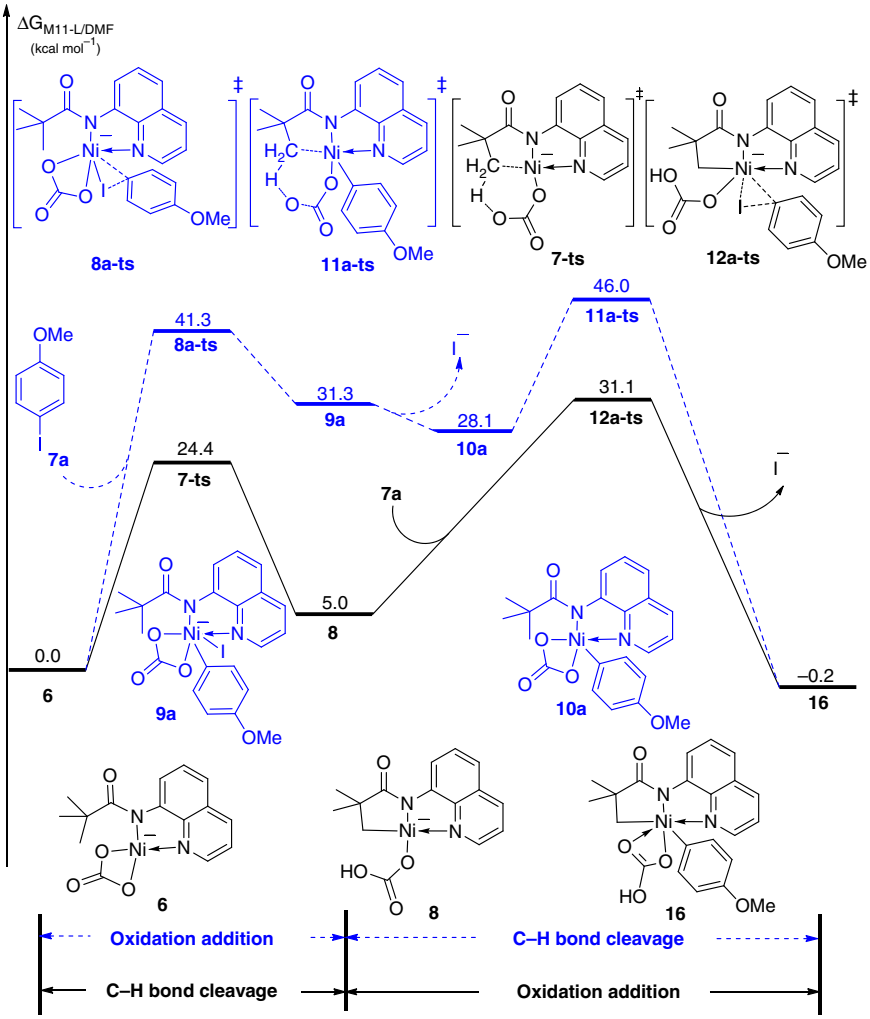

Fig. 9 Free energy of C–H metalation with phenyliodide. The free energy profiles of the C–H bond cleavage and oxidative addition steps during Ni(II)-catalysed C–H bond arylation with a phenyliodide. Relative energy changes are in kcal mol^{-1} and were calculated at the M11-L/6-311+G(d) level in DMF solvent

aryl sources and corresponding Ni intermediates. According to previous theoretical work, electrons are transferred from the d orbital of the Ni centre to the C–I antibonding orbital of the oxidant during oxidative addition of an aryl source to the Ni. As shown in Fig. 10 (see also Supplementary Fig. 3), prior to the C–H bond cleavage step, the highest energy d orbital of Ni in Ni carbonate intermediate **6** is **6-HOMO-1**, which has an energy of −3.04 eV. After C–H bond cleavage, alkyl-Ni intermediate **8** is formed and, due to the electron-donating characteristic of the alkyl group, the energy of the highest energy d orbital of Ni in intermediate **8** (**8-HOMO**) increases to −2.06 eV. The LUMO of phenyliodide **7a** is an antibonding orbital aligned along the C_{aryl}–I bond (**7a-LUMO**). When phenyliodide **7a** is used as the oxidant, the energy of **7a-LUMO** is −1.14 eV, which is 1.90 and 0.92 eV higher in energy than **6-HOMO-1** and **8-HOMO**, respectively. Owing to the higher orbital energy of **8-HOMO**, alkyl-Ni intermediate **8** will more readily donate an electron pair to the phenyliodide **7a** oxidant than Ni carbonate intermediate **6**. Therefore, in this case, carbonate-assisted C–H bond cleavage would be expected to before oxidative addition. In contrast, when cationic diaryliodonium **9′** is used as the oxidant, the energy of the C_{aryl}–I antibonding orbital is only −5.62 eV, which is much lower in energy than **6-HOMO-1** and **8-HOMO**. Thus, both the latter two orbitals can easily donate an electron pair to diaryliodonium **9′**, indicating that the two oxidative addition steps will rapidly proceed in this case. Furthermore, owing to the higher activation free energy associated with C–H bond cleavage in intermediate **6**, oxidative addition will take place prior to carbonate-assisted C–H bond cleavage in this case (Supplementary Fig. 4).

Discussion

DFT calculations with the M11-L functional were performed to determine the mechanisms for the Ni(II)-catalysed C–H arylation of aliphatic amides with either a diaryliodonium salt or a phenyliodide. Interestingly, the reaction pathways were found to be controlled by the molecular orbital level of the oxidant. A common aminonickel intermediate, formed via the coordination and deprotonation–amination of *N*-(quinolinyl)pivalamide with Ni(CO_3) followed by counterion exchange with the carbonate ion, is the active catalyst in the catalytic cycle. However, the subsequent arylation step of this aminonickel intermediate proceeds differently depending on whether a strongly oxidizing diaryliodonium salt or a weakly oxidizing phenyliodide is used. A diaryliodonium salt results in oxidative addition to the active catalyst occurring first, which promotes the subsequent BIES-type C–H bond cleavage step to give an alkyl-aryl-Ni(IV) species. Following this, reductive elimination from the Ni(IV) species forms the new C_{aryl}–C_{alkyl} bond. Finally, the active catalyst is regenerated by

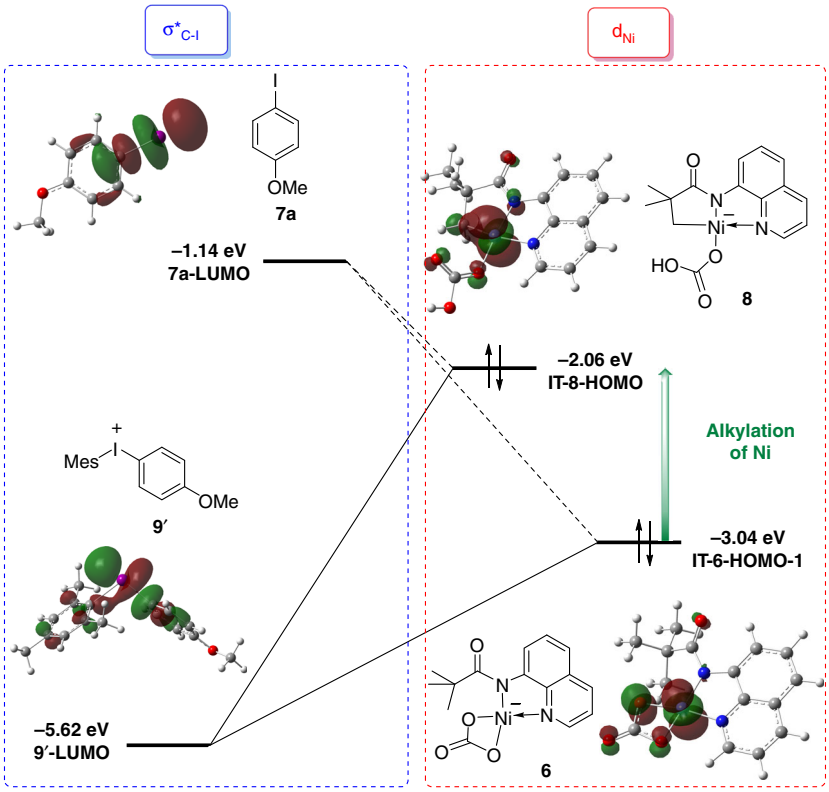

Fig. 10 FMO analysis. FMO analysis of key intermediates during the oxidative addition steps in Ni(II)-catalysed C–H bond arylation. The reacting FMOs of **6**, **8**, **7a**, and **9′** were calculated at the M11-L/6-311+G(d) level

proton exchange with release of the arylation product. The rate-determining step for this pathway is the proton exchange, and the overall activation free energy is 28.8 kcal mol^{-1}. In contrast, the presence of a relatively weak phenyliodide oxidant leads to the reversed reaction sequence: CMD type C–H bond cleavage followed by oxidative addition to give the alkyl-aryl-Ni(IV) species. FMO analysis was employed to study the mechanism associated with the C–H cleavage and oxidative addition. C–H cleavage of the Ni(IV) intermediate was found to proceed via a BIES mechanism, in which the d_{Ni}–σ_{C-H} orbital overlap leads to the generation of a C–Ni bond; while a CMD mechanism is more favourable in the case of a Ni(II) intermediate. The order of the of oxidative addition and carbonate-assisted C–H bond cleavage steps in Ni(II)-catalysed C–H arylation reactions is thus determined by the C_{aryl}–I antibonding orbital level of the oxidant. Owing to the lower energy of the C_{aryl}–I antibonding orbital in a diaryliodonium salt, the oxidative addition step occurs first. Conversely, the relatively high C_{aryl}–I bond antibonding orbital energy of the phenyliodide leads to selective oxidative addition after carbonate-assisted C–H bond cleavage. We believe that this study provides a practical theoretical guide for determining the most important aspects of the oxidant in Ni(II)-catalysed C–H arylation reactions.

Methods

Computational details. All of the DFT calculations were performed with the Gaussian 09 series of programs[58]. The geometries of the different structures were optimized with the B3-LYP functional[59,60] and standard 6–31+G(d) basis set (SDD basis set for Ni and I atoms). Harmonic vibrational frequency calculations were performed for all stationary points to determine whether these were local minima or transition state structures and to derive the thermochemical corrections for the enthalpies and free energies. The M11-L functional[61–64] with the 6–311+G (d) basis set (SDD basis set for Ni and I atoms) was used to calculate the single-point energies and provide highly accurate energy information[65–68]. For the single-point energy calculations, the solvent effect was taken into account by single-point calculations based on the gas-phase stationary points with the SMD[69,70] continuum solvation model. Unless otherwise noted, the experimental solvents used in Figs. 2, 7 were dioxane and *N*,*N*-dimethylformamide (DMF), respectively. All of the three-dimensional molecular diagrams of the molecules were generated with CYLView. The $\Delta G_{M11\text{-}L/solvent}$ values used in the free energy profiles were obtained by eqn 1, in which $\Delta G_{correction/gas}$ is the thermochemical corrections for the gas phas Gibbs free energy calculated at the B3-LYP/6-31+G(d) level in gas phase, and $\Delta E_{M11\text{-}L/solvent}$ is the single-point energy calculated at the M11-L/6-311+G(d) level in the solvent phase based on the gas phase stationary point.

$$\Delta G_{M11-L/solvent} = \Delta E_{M11-L/solvent} + \Delta G_{correction/gas} \quad (1)$$

Data availability

All data generated or analysed during this study are included in this published article (and its supplementary information files) and are available from the corresponding author upon reasonable request. Calculation energies, enthalpies, and free energies are available in Supplementary Data 1. Calculated geometries for optimised compounds and transition states are available in Supplementary Data 2.

Received: 28 September 2018 Accepted: 21 February 2019
Published online: 13 March 2019

References

1. Ackermann, L. Carboxylate-assisted transition-metal-catalyzed C-H bond functionalizations: mechanism and scope. *Chem. Rev.* **111**, 1315–1345 (2011).
2. Balcells, D., Clot, E. & Eisenstein, O. C-H bond activation in transition metal species from a computational perspective. *Chem. Rev.* **110**, 749–823 (2010).
3. He, J., Wasa, M., Chan, K. S. L., Shao, Q. & Yu, J. Q. Palladium-catalyzed transformations of alkyl C-H bonds. *Chem. Rev.* **117**, 8754–8786 (2017).
4. Li, B. & Dixneuf, P. H. sp2 C-H bond activation in water and catalytic cross-coupling reactions. *Chem. Soc. Rev.* **42**, 5744–5767 (2013).
5. Sperger, T., Sanhueza, I. A., Kalvet, I. & Schoenebeck, F. Computational studies of synthetically relevant homogeneous organometallic catalysis

involving Ni, Pd, Ir, and Rh: an overview of commonly employed DFT methods and mechanistic insights. *Chem. Rev.* **115**, 9532–9586 (2015).
6. Wencel-Delord, J. & Glorius, F. C-H bond activation enables the rapid construction and late-stage diversification of functional molecules. *Nat. Chem.* **5**, 369–375 (2013).
7. Engle, K. M., Mei, T. S., Wasa, M. & Yu, J. Q. Weak coordination as a powerful means for developing broadly useful C-H functionalization reactions. *Acc. Chem. Res.* **45**, 788–802 (2012).
8. Sigman, M. S. & Werner, E. W. Imparting catalyst control upon classical palladium-catalyzed alkenyl C-H bond functionalization reactions. *Acc. Chem. Res.* **45**, 874–884 (2012).
9. Wang, X., Gensch, T., Lerchen, A., Daniliuc, C. G. & Glorius, F. Cp*Rh(III)/bicyclic olefin cocatalyzed C-H bond amidation by intramolecular amide transfer. *J. Am. Chem. Soc.* **139**, 6506–6512 (2017).
10. Xie, F., Zhang, Z., Yu, X., Tang, G. & Li, X. Diaryliodoniums by Rhodium(III)-catalyzed C-H activation: mild synthesis and diversified functionalizations. *Angew. Chem. Int. Ed.* **54**, 7405–7409 (2015).
11. Xu, Y., Young, M. C. & Dong, G. Catalytic coupling between unactivated aliphatic C-H bonds and alkynes via a metal-hydride pathway. *J. Am. Chem. Soc.* **139**, 5716–5719 (2017).
12. Murphy, J. M., Lawrence, J. D., Kawamura, K., Incarvito, C. & Hartwig, J. F. Ruthenium-catalyzed regiospecific borylation of methyl C-H bonds. *J. Am. Chem. Soc.* **128**, 13684–13685 (2006).
13. Simonetti, M. et al. Ru-catalyzed C-H arylation of fluoroarenes with aryl halides. *J. Am. Chem. Soc.* **138**, 3596–3606 (2016).
14. Hong, X., Liang, Y. & Houk, K. N. Mechanisms and origins of switchable chemoselectivity of Ni-catalyzed C(aryl)-O and C(acyl)-O activation of aryl esters with phosphine ligands. *J. Am. Chem. Soc.* **136**, 2017–2025 (2014).
15. Muto, K., Yamaguchi, J. & Itami, K. Nickel-catalyzed C-H/C-O coupling of azoles with phenol derivatives. *J. Am. Chem. Soc.* **134**, 169–172 (2012).
16. Rosen, B. M. et al. Nickel-catalyzed cross-couplings involving carbon-oxygen bonds. *Chem. Rev.* **111**, 1346–1416 (2011).
17. Yao, T., Hirano, K., Satoh, T. & Miura, M. Nickel- and cobalt-catalyzed direct alkylation of azoles with N-tosylhydrazones bearing unactivated alkyl groups. *Angew. Chem. Int. Ed.* **51**, 775–779 (2012).
18. Rouquet, G. & Chatani, N. Catalytic functionalization of C(sp2)-H and C(sp3)-H bonds by using bidentate directing groups. *Angew. Chem. Int. Ed.* **52**, 11726–11743 (2013).
19. Tasker, S. Z., Standley, E. A. & Jamison, T. F. Recent advances in homogeneous nickel catalysis. *Nature* **509**, 299–309 (2014).
20. Ananikov, V. P. Nickel: the "Spirited Horse" of transition metal catalysis. *ACS Catal.* **5**, 1964–1971 (2015).
21. Heinemann, C., Hertwig, R. H., Wesendrup, R., Koch, W. & Schwarz, H. Relativistic effects on bonding in cationic transition-metal-carbene complexes: a density-functional study. *J. Am. Chem. Soc.* **117**, 495–500 (1995).
22. Uddin, J., Morales, C. M., Maynard, J. H. & Landis, C. R. Computational studies of metal−ligand bond enthalpies across the transition metal series. *Organometallics* **25**, 5566–5581 (2006).
23. Xie, H., Sun, Q., Ren, G. & Cao, Z. Mechanisms and reactivity differences for cycloaddition of anhydride to alkyne catalyzed by palladium and nickel catalysts: insight from density functional calculations. *J. Org. Chem.* **79**, 11911–11921 (2014).
24. Shiota, H., Ano, Y., Aihara, Y., Fukumoto, Y. & Chatani, N. Nickel-catalyzed chelation-assisted transformations involving ortho C-H bond activation: regioselective oxidative cycloaddition of aromatic amides to alkynes. *J. Am. Chem. Soc.* **133**, 14952–14955 (2011).
25. Aihara, Y. & Chatani, N. Nickel-catalyzed direct alkylation of C-H bonds in benzamides and acrylamides with functionalized alkyl halides via bidentate-chelation assistance. *J. Am. Chem. Soc.* **135**, 5308–5311 (2013).
26. Aihara, Y. & Chatani, N. Nickel-catalyzed reaction of C–H bonds in amides with I2: ortho-Iodination via the cleavage of C(sp2)–H bonds and oxidative cyclization to β-lactams via the cleavage of C(sp3)–H bonds. *ACS Catal.* **6**, 4323–4329 (2016).
27. Aihara, Y., Tobisu, M., Fukumoto, Y. & Chatani, N. Ni(II)-catalyzed oxidative coupling between C(sp(2))-H in benzamides and C(sp(3))-H in toluene derivatives. *J. Am. Chem. Soc.* **136**, 15509–15512 (2014).
28. Kubo, T. & Chatani, N. Dicumyl peroxide as a methylating reagent in the Ni-catalyzed methylation of ortho C-H bonds in aromatic amides. *Org. Lett.* **18**, 1698–1701 (2016).
29. Landge, V. G. et al. Nickel-catalyzed direct alkynylation of C(sp2)–H bonds of amides: an "inverse Sonogashira strategy" to ortho-alkynylbenzoic acids. *Catal. Sci. Technol.* **6**, 1946–1951 (2016).
30. Lin, C. et al. Nickel-catalyzed direct thioetherification of beta-C(sp(3))-H bonds of aliphatic amides. *Org. Lett.* **17**, 1340–1343 (2015).
31. Liu, Y. J., Liu, Y. H., Yan, S. Y. & Shi, B. F. A sustainable and simple catalytic system for direct alkynylation of C(sp(2))-H bonds with low nickel loadings. *Chem. Commun.* **51**, 6388–6391 (2015).
32. Maity, S., Agasti, S., Earsad, A. M., Hazra, A. & Maiti, D. Nickel-catalyzed insertion of alkynes and electron-deficient olefins into unactivated sp(3) C-H bonds. *Chem. -Eur. J.* **21**, 11320–11324 (2015).
33. Ruan, Z., Lackner, S. & Ackermann, L. A general strategy for the nickel-catalyzed C-H alkylation of anilines. *Angew. Chem. Int. Ed.* **55**, 3153–3157 (2016).
34. Wang, X. et al. Nickel-catalyzed direct C (sp(3))-H arylation of aliphatic amides with thiophenes. *Org. Lett.* **17**, 5228–5231 (2015).
35. Wu, X., Zhao, Y. & Ge, H. Nickel-catalyzed site-selective alkylation of unactivated C(sp3)-H bonds. *J. Am. Chem. Soc.* **136**, 1789–1792 (2014).
36. Yang, K. et al. Nickel-catalyzed and benzoic acid-promoted direct sulfenylation of unactivated arenes. *Chem. Commun.* **51**, 3582–3585 (2015).
37. Ye, X., Petersen, J. L. & Shi, X. Nickel-catalyzed directed sulfenylation of sp(2) and sp(3) C-H bonds. *Chem. Commun.* **51**, 7863–7866 (2015).
38. Yi, J., Yang, L., Xia, C. & Li, F. Nickel-catalyzed alkynylation of a C(sp(2))-H bond directed by an 8-aminoquinoline moiety. *J. Org. Chem.* **80**, 6213–6221 (2015).
39. Aihara, Y. & Chatani, N. Nickel-catalyzed direct arylation of C(sp3)-H bonds in aliphatic amides via bidentate-chelation assistance. *J. Am. Chem. Soc.* **136**, 898–901 (2014).
40. Iyanaga, M., Aihara, Y. & Chatani, N. Direct arylation of C(sp3)-H bonds in aliphatic amides with diaryliodonium salts in the presence of a nickel catalyst. *J. Org. Chem.* **79**, 11933–11939 (2014).
41. Kim, D. S., Park, W. J. & Jun, C. H. Metal-organic cooperative catalysis in C-H and C-C bond activation. *Chem. Rev.* **117**, 8977–9015 (2017).
42. Li, Y., Zou, L., Bai, R. & Lan, Y. Ni(i)–Ni(iii) vs. Ni(ii)–Ni(iv): mechanistic study of Ni-catalyzed alkylation of benzamides with alkyl halides. *Org. Chem. Front.* **5**, 615–622 (2018).
43. Liu, S., Qi, X., Qu, L.-B., Bai, R. & Lan, Y. C–H bond cleavage occurring on a Rh(v) intermediate: a theoretical study of Rh-catalyzed arene azidation. *Catal. Sci. Technol.* **8**, 1645–1651 (2018).
44. Qi, X., Li, Y., Bai, R. & Lan, Y. Mechanism of rhodium-catalyzed C-H functionalization: advances in theoretical investigation. *Acc. Chem. Res.* **50**, 2799–2808 (2017).
45. Tan, G., Zhu, L., Liao, X., Lan, Y. & You, J. Rhodium/copper cocatalyzed highly trans-selective 1,2-diheteroarylation of alkynes with azoles via C-H addition/oxidative cross-coupling: a combined experimental and theoretical study. *J. Am. Chem. Soc.* **139**, 15724–15737 (2017).
46. Zhang, T. et al. Computational investigation of the role played by rhodium(V) in the rhodium(III)-catalyzed ortho-bromination of arenes. *Chem. -Eur. J.* **23**, 2690–2699 (2017).
47. Zhou, X. et al. Cp*CoIII-catalyzed branch-selective hydroarylation of alkynes via C–H activation: efficient access to α-gem-vinylindoles. *ACS Catal.* **7**, 7296–7304 (2017).
48. Zhu, L. et al. Ir(III)/Ir(V) or Ir(I)/Ir(III) Catalytic Cycle? Steric-effect-controlled mechanism for the para-C–H borylation of arenes. *Organometallics* **36**, 2107–2115 (2017).
49. Lin, Y., Zhu, L., Lan, Y. & Rao, Y. Development of a rhodium(II)-catalyzed chemoselective C(sp(3))-H oxygenation. *Chem. -Eur. J.* **21**, 14937–14942 (2015).
50. O'Duill, M. L. et al. Tridentate directing groups stabilize 6-membered palladacycles in catalytic alkene hydrofunctionalization. *J. Am. Chem. Soc.* **139**, 15576–15579 (2017).
51. Omer, H. M. & Liu, P. Computational study of Ni-catalyzed C-H functionalization: factors that control the competition of oxidative addition and radical pathways. *J. Am. Chem. Soc.* **139**, 9909–9920 (2017).
52. Singh, S., K, S. & Sunoj, R. B. Aliphatic C(sp(3))-H bond activation using nickel catalysis: mechanistic insights on regioselective arylation. *J. Org. Chem.* **82**, 9619–9626 (2017).
53. Barsu, N., Kalsi, D. & Sundararaju, B. Carboxylate assisted Ni-catalyzed C-H bond allylation of benzamides. *Chem. -Eur. J.* **21**, 9364–9368 (2015).
54. Haines, B. E., Yu, J. Q. & Musaev, D. G. The mechanism of directed Ni(ii)-catalyzed C-H iodination with molecular iodine. *Chem. Sci.* **9**, 1144–1154 (2018).
55. Wang, X. et al. Nickel-catalyzed direct thiolation of C(sp(3))-H bonds in aliphatic amides. *Org. Lett.* **17**, 1970–1973 (2015).
56. Bu, Q., Rogge, T., Kotek, V. & Ackermann, L. Distal weak coordination of acetamides in ruthenium(II)-catalyzed C–H activation processes. *Angew. Chem. Int. Ed.* **57**, 765–768 (2018).
57. Oxgaard, J., Tenn, W. J., Nielsen, R. J., Periana, R. A. & Goddard, W. A. Mechanistic analysis of iridium heteroatom C−H activation: evidence for an internal electrophilic substitution mechanism. *Organometallics* **26**, 1565–1567 (2007).
58. Frisch, M. J. T., et al. Gaussian 09; Gaussian, Inc.: Wallingford, CT, 2013.
59. Becke, A. D. Density-functional thermochemistry. III. The role of exact exchange. *J. Chem. Phys.* **98**, 5648–5652 (1993).
60. Lee, C., Yang, W. & Parr, R. G. Development of the Colle-Salvetti correlation-energy formula into a functional of the electron density. *Phys. Rev. B.* **37**, 785–789 (1988).
61. Hopmann, K. H. How accurate is DFT for iridium-mediated chemistry? *Organometallics* **35**, 3795–3807 (2016).

62. Peverati, R. & Truhlar, D. G. Improving the accuracy of hybrid meta-GGA density functionals by range separation. *J. Phys. Chem. Lett.* **2**, 2810–2817 (2011).
63. Peverati, R. & Truhlar, D. G. M11-L: a local density functional that provides improved accuracy for electronic structure calculations in chemistry and physics. *J. Phys. Chem. Lett.* **3**, 117–124 (2011).
64. Zhu, L., Qi, X. & Lan, Y. Rhodium-catalyzed hetero-(5+2) cycloaddition of vinylaziridines and alkynes: a theoretical view of the mechanism and chirality transfer. *Organometallics* **35**, 771–777 (2016).
65. Lin, Y. S., Tsai, C. W., Li, G. D. & Chai, J. D. Long-range corrected hybrid meta-generalized-gradient approximations with dispersion corrections. *J. Chem. Phys.* **136**, 154109 (2012).
66. Peverati, R. & Truhlar, D. G. Performance of the M11 and M11-L density functionals for calculations of electronic excitation energies by adiabatic time-dependent density functional theory. *Phys. Chem. Chem. Phys.* **14**, 11363–11370 (2012).
67. Steckel, J. A. Ab initio calculations of the interaction between CO_2 and the acetate ion. *J. Phys. Chem. A* **116**, 11643–11650 (2012).
68. Zhao, Y., Ng, H. T., Peverati, R. & Truhlar, D. G. Benchmark database for ylidic bond dissociation energies and its use for assessments of electronic structure methods. *J. Chem. Theory Comput.* **8**, 2824–2834 (2012).
69. Cancès, E., Mennucci, B. & Tomasi, J. A new integral equation formalism for the polarizable continuum model: theoretical background and applications to isotropic and anisotropic dielectrics. *J. Chem. Phys.* **107**, 3032–3041 (1997).
70. Cossi, M., Barone, V., Cammi, R. & Tomasi, J. Ab initio study of solvated molecules: a new implementation of the polarizable continuum model. *Chem. Phys. Lett.* **255**, 327–335 (1996).

Acknowledgements

This project was supported by the National Science Foundation of China (Grants 21822303 and 21772020) and Fundamental Research Funds for the Central Universities (Chongqing University) (No. 2018CDXZ0002; 2018CDPTCG0001/4).

Author contributions

T.Z., S.L., L.Z., R.B. and Y.L. conceived the project and analysed the computational results. T.Z., F.L., K.Z. and Y.Z. performed the theoretical calculations. R.B. and Y.L. composed the manuscript with input from all authors.

Additional information

Supplementary information accompanies this paper at https://doi.org/10.1038/s42004-019-0132-5.

Competing interests: The authors declare no competing interests.

Reprints and permission information is available online at http://npg.nature.com/reprintsandpermissions/

Publisher's note: Springer Nature remains neutral with regard to jurisdictional claims in published maps and institutional affiliations.

Open Access This article is licensed under a Creative Commons Attribution 4.0 International License, which permits use, sharing, adaptation, distribution and reproduction in any medium or format, as long as you give appropriate credit to the original author(s) and the source, provide a link to the Creative Commons license, and indicate if changes were made. The images or other third party material in this article are included in the article's Creative Commons license, unless indicated otherwise in a credit line to the material. If material is not included in the article's Creative Commons license and your intended use is not permitted by statutory regulation or exceeds the permitted use, you will need to obtain permission directly from the copyright holder. To view a copy of this license, visit http://creativecommons.org/licenses/by/4.0/.

© The Author(s) 2019